Spatial chaos and patterns in laser-produced plasmas

Cangtao Zhou and X. T. He
China Center of Advanced Science and Technology (World Laboratory), P.O. Box 8730, Beijing 100080, China
and Laboratory of Computational Physics and Center for Nonlinear Studies,
*Institute of Applied Physics and Computational Mathematics, P.O. Box 8009, Beijing 100088, China**
(Received 20 July 1993)

Spatial chaos and patterns of laser beams in plasmas are investigated in terms of a saturable nonlinear Schrödinger equation, theoretically and numerically. The linear analysis shows that the homoclinic orbit crossings may exist in phase space, which is also verified in our numerical experiments. In particular, current research illustrates that the spatial chaos and complicated patterns of light wave interacting with plasmas arise from the high order saturable nonlinear effects. The complicated patterns are associated with the stochastic partition of energy contained in Fourier modes. In addition, some physical significance for our work has been discussed.

PACS number(s): 52.35.Mw, 47.10.+g, 05.45.+b, 52.40.Db

I. INTRODUCTION

In laser-plasma interaction, considering the Maxwell equations and the motion equations of an electron, one can obtain the wave equation for the light electric fields [1,2],

$$2ik_0c^2\frac{\partial E}{\partial z}+c^2\nabla_\perp^2E+\omega_{p0}^2\frac{\delta n}{n_0}E=0\ , \tag{1.1}$$

and the fluid equation of the electron density,

$$\frac{\partial^2}{\partial t^2}l_nn-c_s^2\nabla_\perp^2l_nn=\nabla_\perp^2c_s^2+\frac{Ze^2}{4m_em_i}\nabla_\perp^2|E|^2\ , \tag{1.2}$$

where $c_s=\sqrt{(ZT_e+T_i)/m_i}$ is the acoustic velocity, c is the light velocity, $n\equiv n_0-\delta n$, n_0 is the unperturbed electron density, k_0 is the laser wave number, ω_{p0} is the plasma frequency, and T_e,T_i and m_e,m_i represent the electron and ion temperature and mass, respectively.

In the static approximation, Eqs. (1.1) and (1.2) are reduced to the nonlinear Schrödinger equation (NSE) [3–6]

$$2ik_0c^2\frac{\partial E}{\partial z}+c^2\nabla_\perp^2E+\omega_{p0}^2(1-e^{-\beta|E|^2})E=0\ , \tag{1.3}$$

where $\beta=e^2/4m_e\omega_{p0}^2T_e(1+T_i/ZT_e)$. Equation (1.3) obviously describes the case where a light beam propagates in a steady state, but varies in space. In other words, the ponderomotive force completely dominates ion inertia, and must be balanced by pressure forces instead.

For the dynamic model (1.3), the self-focusing, self-trapped, and laser beam filamentations due to the ponderomotive force in plasmas were extensively studied. Max [3] showed that the self-focusing becomes a periodic oscillatory phenomenon, rather than a catastrophic process due to the exponential nonlinearity. Lam, Lippmann, and Tappert [4] illustrated that the self-trapped beams are stable. Kaw, Schmidt, and Wilcox [5] showed that an electromagnetic wave interacting with a plasma is subject to instabilities leading to filamentation. Johnston [6] numerically discussed the fast and slow filamentations in plasmas.

Considering many physical applications, here we rewrite Eq. (1.3) as a more generally one-dimensional dimensionless form,

$$i\frac{\partial E}{\partial z}+\frac{\partial^2E}{\partial x^2}+\frac{1}{2g}(1-e^{-2g|E|^2})E=0\ , \tag{1.4}$$

where g is the parameter. When $g=0$, Eq. (1.4) becomes the well-known cubic NSE, which is integrable due to the existence of the Lax pair. A class of periodic solutions and solitons can be obtained by the inverse scattering transform.

Although the self-focusing and filamentation phenomena have been extensively discussed, as we know, another important dynamic behavior for Eq. (1.3) or Eq. (1.4) to describe, the laser beam propagation (spatial chaos) has not been studied in detail. Our main purpose here is to investigate the spatial patterns of laser beams interacting with plasmas. In addition, the integrable problem of Eq. (1.4) is discussed. In Sec. II, we simply analyze the periodic solution of Eq. (1.4) and give the linear discussions. The spatial chaos and patterns are described in Secs. III and IV, respectively, and some summaries and discussions are given in the final section.

II. QUALITATIVE ANALYSES

A. Traveling-wave solution

For Eq. (1.4), we assume

$$E(x,z)=G(\xi)e^{i[(v/2)x-\Omega Z]}\ , \tag{2.1}$$

where $\xi=x-vz$. Inserting Eq. (2.1) into Eq. (1.4) and integrating once, we yield

$$\frac{1}{2}\left[\frac{dG}{d\xi}\right]^2+V(G)=H_0\ , \tag{2.2}$$

*Mailing address.

where H_0 is the integration constant that represents the pseudoenergy, and the pseudopotential $V(G)$ is

$$V(G)=\frac{1}{8g^2}(e^{-2gG^2}-1)+\left[\frac{1}{4g}-\frac{\alpha^2}{2}\right]G^2 , \tag{2.3}$$

where $\alpha^2=v^2/4-\Omega$, which is plotted in Fig. 1. Equation (2.2) can be considered as an energy integral of a classical particle with unit mass. We know from the classical mechanics that the particle motion is periodic if a particle lies in the potential well ($H_0<0$), and the solution corresponds to a periodic one. As $H_0=0$, the solution corresponds to a solitary, where the strength and the characteristic width of the laser beams can be given when we obtain such a solution [7]. However, the explicitly analytical solitary has not been obtained as yet, which is due to the complication of the potential function (2.3).

B. Linearized analysis

On the other hand, a simpler homogeneous solution can be written as

$$E_s(z)=E_0e^{iz} , \tag{2.4}$$

where

$$E_0=0 , \quad \pm\left[\frac{1}{2g}l_n(1-2g)^{-1}\right]^{1/2} \tag{2.5}$$

for $0\le g<\frac{1}{2}$. We assume the initial state to be E_0. Now let us analyze the developed behavior for such an initial state. Defining

$$E(x,z)=E_s(z)+\delta E(x,z) \tag{2.6}$$

and linearizing Eq. (1.4) as done in Ref. [8], we easily obtain

$$\left.\frac{\delta E}{\delta E^*}\right|_{z=0}=\pm i \tag{2.7}$$

and

$$|\delta E(x,z)|=c_1e^{Az}\cos(K_{\max}x)+c_2e^{-Az}\cos(K_{\max}x) \tag{2.8}$$

for $E_0=\sqrt{(1/2g)l_n(1-2g)^{-1}}$ with $0\le g<\frac{1}{2}$,

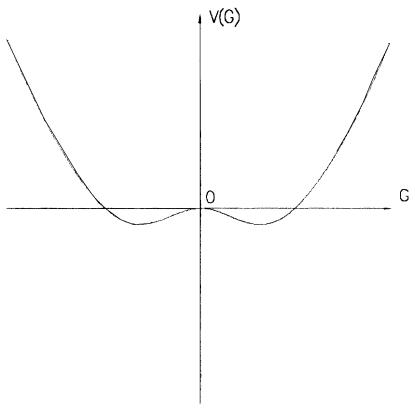

FIG. 1. The pseudopotential function (2.3).

where c_1 and c_2 are the small parameters, $A=[(1/2g)-1]l_n(1-2g)$, and $K_{\max}$ represents the maximum instability wave number. If we construct the phase space as $(|E(x,z)|,d|E(x,z)|/dz)$, then $[\sqrt{(1/2g)l_n(1-2g)^{-1}}, 0]$ corresponds to a saddle point in phase space. Owing to the integrability of the cubic NSE, on the other hand, the orbits that pass the saddle point (1,0) must be the homoclinic orbits (HMO's) [9].

III. SPATIAL CHAOS AND ITS DESCRIPTIONS

From steady-state analysis, we know the linear developed behavior of the homogeneous solution. A further discussion will be finished by using the numerical experiments.

According to the results obtained in Sec. II B, on the other hand, we take the initial condition as

$$E(x,0)=E_0+\epsilon e^{i\theta}\cos(K_{\max}x) , \tag{3.1}$$

where ϵ is a real parameter and $E_0=\sqrt{(1/2g)l_n(1-2g)^{-1}}$. In numerical processes, the periodic length of the system is taken as $L=2\pi/K_{\max}$, and the standard splitting-step spectral method [10] has been improved in order to increase the accuracy, which depends on the accuracy of conserved quantities being preserved to 10^{-8}.

In order to analyze the chaotic properties of the saturable NSE (1.4), we first discuss the behavior of the HMO crossings. In Sec. II B, we show that $(E_0,0)$ [where $E_0=\sqrt{(1/2g)l_n(1-2g)^{-1}}$] corresponds to a saddle point in phase space. Comparing Eqs. (2.6) and (2.7) with the initial condition (3.1), we easily determine that the unstable manifolds for possessing the saddle point $(E_0,0)$ correspond to $\theta=45°$ and 225°, and the stable manifolds correspond to $\theta=135°$ and 315°.

As far as a finite dimensional dynamic system is concerned, the stable and unstable orbits for the hyperbolic fixed point would be smoothly joined to each other if the unperturbed system were taken to be integrable. For a Hamiltonian perturbation, the orbits generically intersect transversely, leading to an infinite number of homoclinic points and chaotic motion [11]. According to this idea, we also deal with our continuum Hamiltonian system. As $g=0$, the stable and unstable manifolds that possess the saddle point (1,0) should be smoothly joined to each other due to the integrability of the cubic NSE. Making use of the results obtained in the linear stability analysis, we choose the initial parameters as $\epsilon=0.0001$, $\theta=45°$, and consider two cases of $g=0$ and $g=0.1$, respectively. From Fig. 2(a), we observe that the stable manifold $W^{(s)}$ smoothly joins with the unstable manifold $W^{(u)}$. The orbit that possesses the saddle point (1, 0) corresponds to the homoclinic one. As $g\neq0$, however, we find that the stable and unstable manifolds in phase space do not smoothly join together as shown in Fig. 2(b), which illustrates that the current system is near integrable. It is also noted that there are not an infinite number of homoclinic points in Fig. 2(b). In fact, our phase space $(|E(x,z)|,d|E(x,z)|/dz)$ is only the projection of a high-dimensional space, where the information of phase

for wave fields is not considered. Therefore, there may exist some difference between our HMO crossings with those in a finite-dimensional Hamiltonian system in which the infinite homoclinic points appear.

To analyze the spatial chaos, we further discuss the propagative behavior of wave fields. Here, we choose an initial position that lies in the nearby saddle point $(E_0,0)$, that is, $\epsilon=0.1$, $\theta=45.225°$. For $g=0$, the integrability for the cubic NSE can be seen from our previous work [8], where the amplitude of wave fields propagates periodically. The exactly periodic recurrent solution is also exhibited in Fig. 3(a). For $g=0.1$, however, a completely different dynamic behavior is shown in Fig. 3(b). We observe that the localized structures are still kept in the propagative processes of wave fields. The presence of these complicated patterns shows the coherence broken down. To better analyze the propagative characteristic of wave fields, we trace a fixed position in x space. As shown in Fig. 4, the typically chaotic characteristic has been described. As for wave fields, the amplitude, $|E(x,z)|$ experiences the stochastic oscillation at sufficiently far distances [see Fig. 4(b)]. In particular, the irregular HMO crossings as exhibited in Fig. 4(a) are very clear. A continuous nonperiodic spectrum is described in Fig. 4(c). From these figures, we believe that the wave fields are stochastic propagation, which arises from the Hamiltonian perturbation

$$H_1=\int\left\{\frac{1}{4}|E|^4-\frac{1}{2g}\left[|E|^2+\frac{1}{2g}(e^{-2g|E|^2}-1\right]\right\}dx\ . \tag{3.2}$$

To illustrate the route to spatial chaos, we fix parameters $\theta=45.225°$, $\epsilon=0.1$ and vary g. From Fig. 5, we find the foundational frequency $\omega_0=0.2513$ for $g=0$. When $g=0.0002$, the wave field still seems to propagate with periodic behavior, but some small peaks in the power spectrum appear and the base frequencies are not uniquely defined (see Table I). When $g=0.0008$, in particular, more peaks are produced (but still countable), although the solution does not recur within the finite distance. In

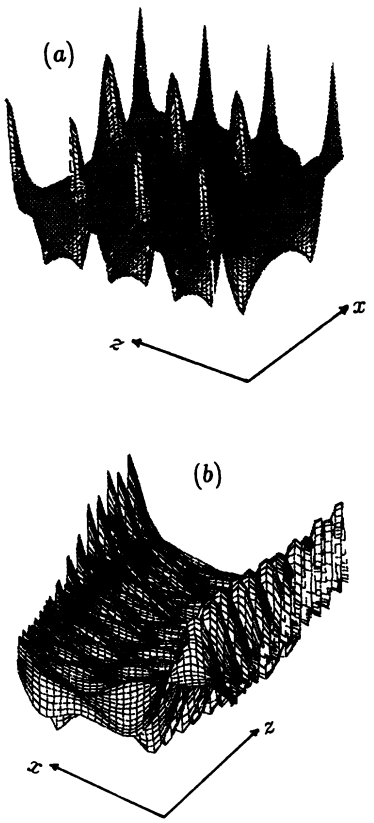

FIG. 3. Envelope amplitude of Eq. (1.4), with $\epsilon=0.1$ and $\theta=45.225°$. (a) $g=0$. (b) $g=0.1$.

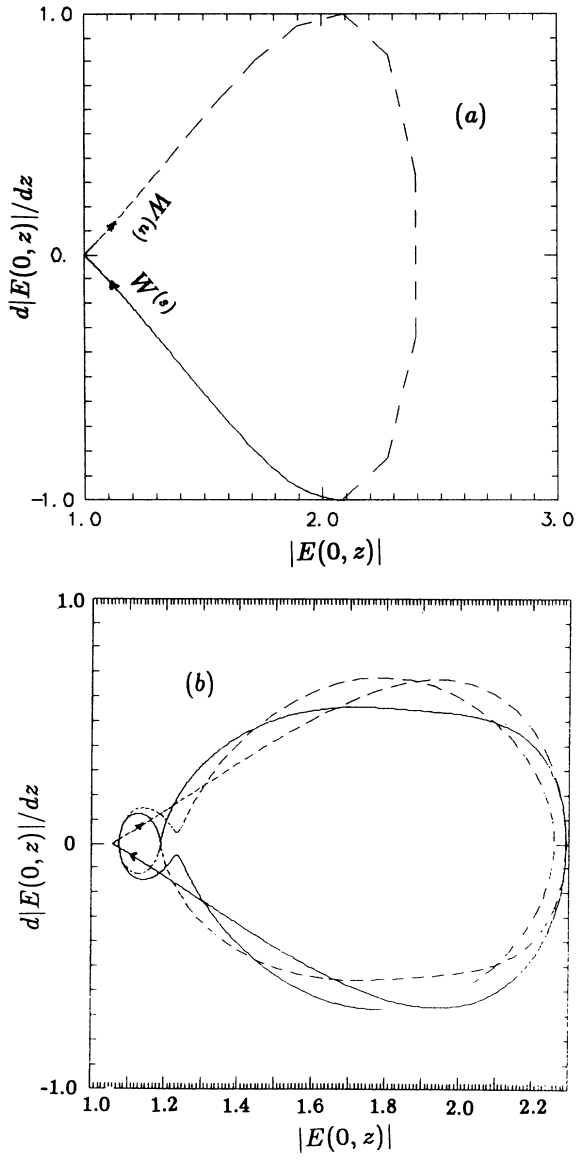

FIG. 2. Stable ($W^{(s)}$) and unstable ($W^{(u)}$) manifolds for the hyperbolic fixed point $[\sqrt{(1/2g)l_n(1-2g)^{-1}},0]$, where the point line is computed with $z>0$ and the solid line is computed with $z<0$. (a) Integrable cubic NSE; the orbits smoothly join. (b) Nonintegrable saturable NSE (1.4) with $g=0.1$.

a sense, these solutions are called quasiperiodic solutions [12]. To demonstrate this conclusion, we should discuss the definition of a quasiperiodic solution. As a matter of fact, a quasiperiodic solution is one that can be expressed as a countable sum of periodic functions with the following two properties: (i) it is linear independent; and (ii) it forms a finite integral base for the frequency. From Fig. 5 and Table I, we see that the countable frequencies do exist. In special cases, we find that the phase-space trajectory, the wave form of $|E(x,z)|$, and the spectrum of the wave form are completely similar to those cases reported in Ref. [12], in which the quasiperiodic solutions of the Ver Pol equation are described. Of course, owing to the impossibility of determining whether a measured value is rational or irrational numerically, a spectrum that appears to be quasiperiodic may actually be periodic with an extremely long periodic solution (see Fig. 5 for $g=0.0002$). On the other hand, with the increase of parameter g, the continuous power spectrum reveals the chaotic behavior (see Fig. 5, in the case of $g=0.01$, and Fig. 4). In addition, we also measure the maximum Lyapunov exponent. It is seen from Fig. 6 that the maximum Lyapunov exponent is positive for the large parts of parametric g. Therefore, the spatial chaos is the main characteristic of the current Hamiltonian system.

Here, we simply illustrate the forming mechanism for the appearance of our spatial chaos. From the standpoint of nonlinear dynamics, the base frequency of the cubic NSE is unique (ω_0) for our parameter due to the integrability of the system. However, the nonintegrable perturbation H_1 (3.2) will make the frequency shift, that is, $\omega_i=\omega_0+\Delta\omega_i$. When the parameter g is quite small, there exists finite countable frequencies. With the increase of g, the oscillatory overlapping of the modes could occur [13], which leads to the formation of the stochastic layer and the appearance of the continuous power spectrum.

IV. COMPLICATED PATTERNS AND THEIR CHARACTERISTICS

In Sec. III we have shown that nonintegrable perturbation leads to the chaotic propagation of wave fields. Also, the complicated patterns have been described in Fig. 3(b), in which we observe the solitarylike structures to be quite irregular. In fact, these irregular patterns are associated with the partition of energy in Fourier modes. For the cubic NSE, the energy in Fourier modes is homogeneous decay, which leads to the formation of coherent

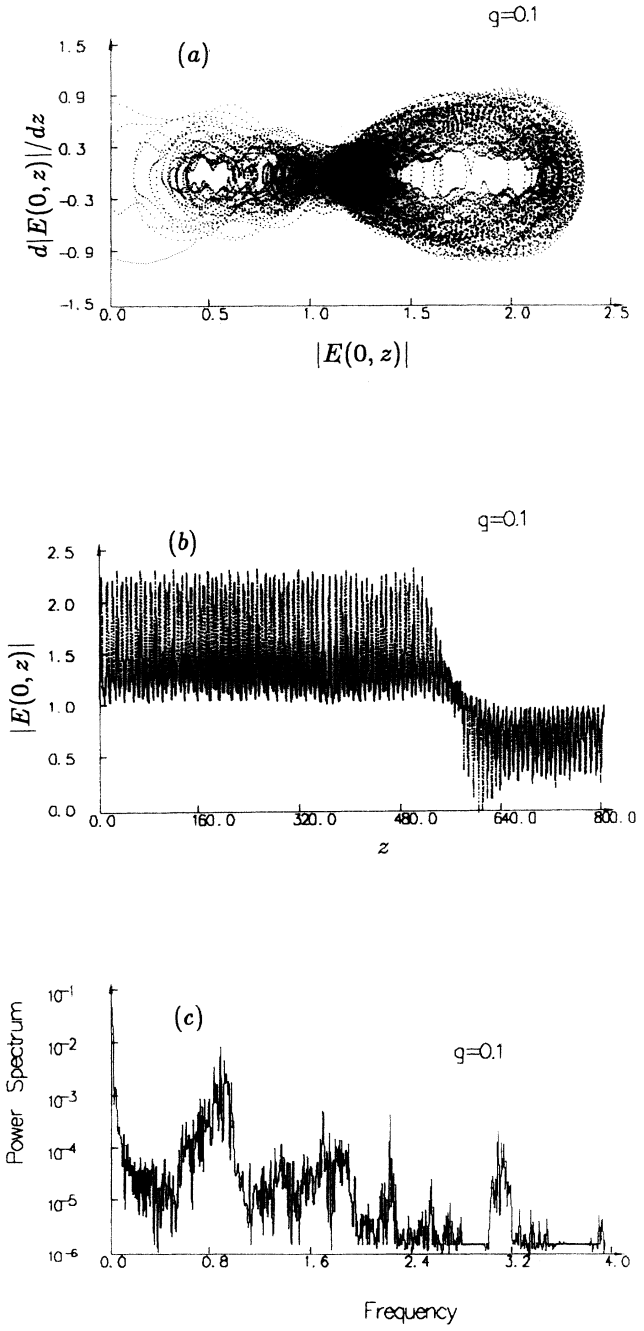

FIG. 4. (a) Phase trajectories illustrate the irregular HMO crossings. (b) Propagation of the field amplitude. (c) Continuous power spectrum shows the chaotic characteristic.

TABLE I. Frequencies corresponding to the high peaks, where p represents the nth high peak. Note that the base frequency for $g=0$ equals 0.251 32, and is about 0.251 33 for $g=0.0002$. However, the "base" frequency for $g=0.0005$ and 0.0008 is not unique, which illustrates that their solutions are quasiperiodic.

g P	1	2	3	4	5	6	7	8	9	10
0.0	0.251 32	0.502 65	0.753 98	1.005 30	1.256 63	1.507 92	1.759 29	2.010 61	2.261 94	2.513 27
0.0002	0.251 33	0.502 65	0.769 69	1.005 31	1.256 64	1.492 256	1.743 584	1.994 921	2.246 238	2.497 566
0.0005	0.235 62	0.486 95	0.722 56	0.989 60	1.240 92	1.476 55	1.712 16	1.979 21	2.214 82	2.497 56
0.0008	0.282 74	0.644 02	1.005 31	1.209 51	1.507 96	1.853 55	2.151 99	2.224 78	2.560 39	2.701 77

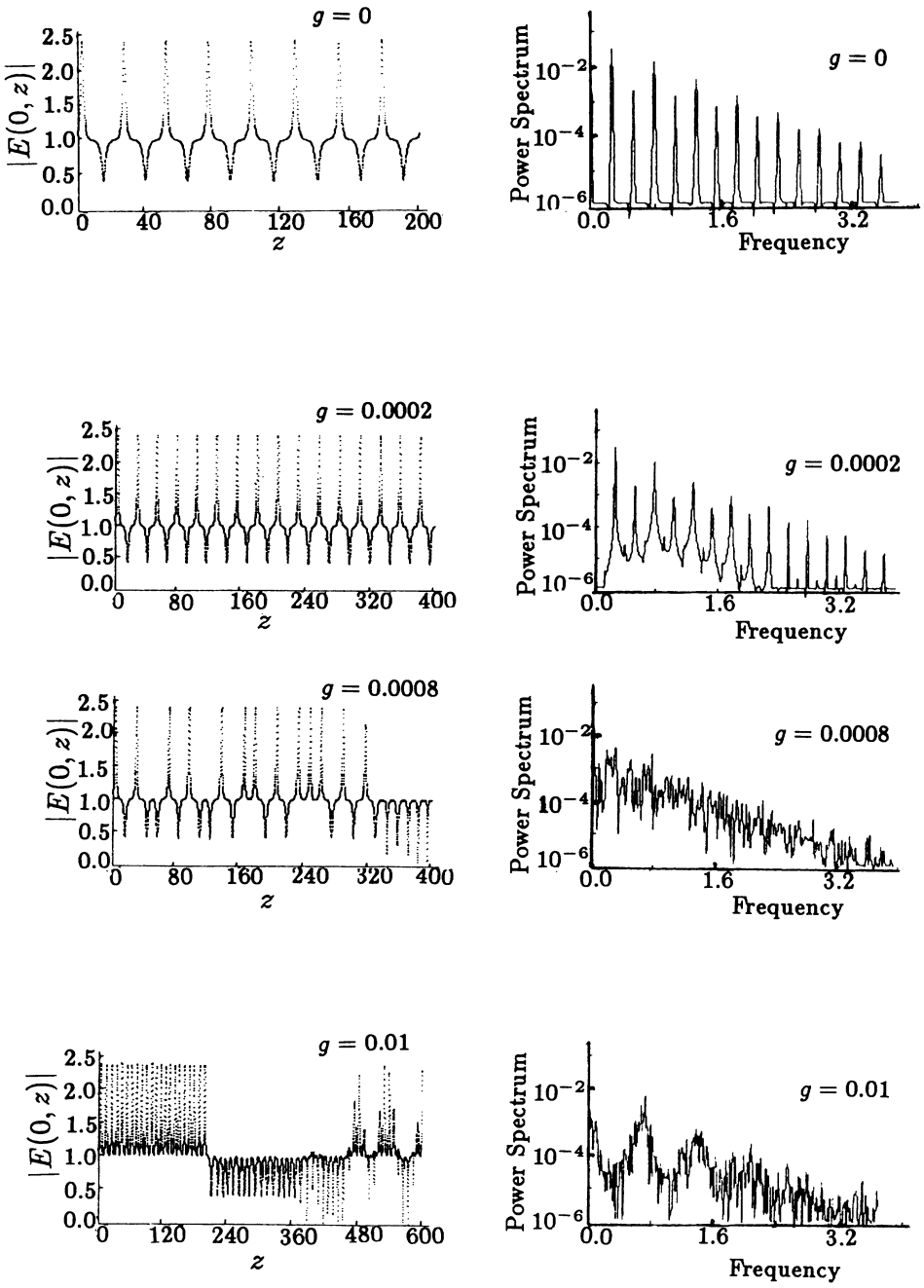

FIG. 5. The periodic solution, quasiperiodic solutions, and chaotic solutions with $\epsilon=0.1$ and $\theta=45.225°$. (a) Propagation of the field amplitude. (b) Power spectrum.

structures. For the saturable NSE (1.4), however, Fig. 7 shows that the partition of energy in Fourier modes is inhomogeneous decay, which results in the localized structures becoming considerably irregular.

To analyze the mechanism that leads to the appearance of the complicated patterns, we further investigate the evolutive process of energy in Fourier modes. For Eq. (1.4), we define the energy of the system as

$$H=\int |E|^2 dx \ . \tag{4.1}$$

In Fourier space, it can be rewritten as

$$H=\sum_n H_{K_n}=\sum_n |E_{K_n}|^2 \ . \tag{4.2}$$

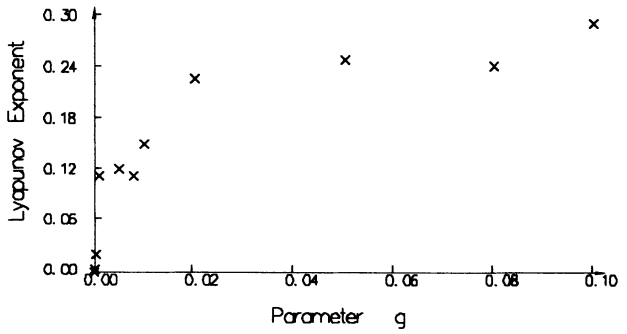

FIG. 6. Lyapunov exponent computed from the series ($|E(0,z)|\sim z$),

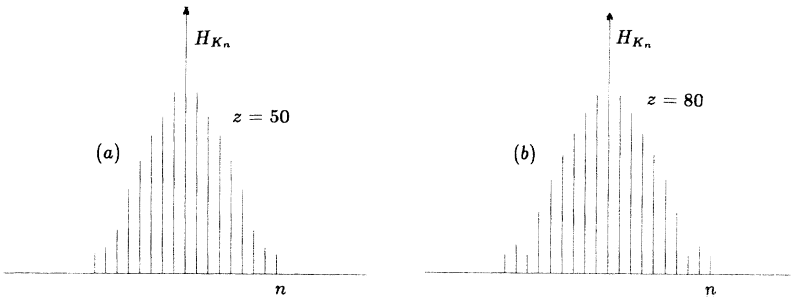

FIG. 7. Energy contained in Fourier modes with the differently propagative distance.

Here K_n stands for the nth Fourier mode. The propagative processes of the amplitude for wave fields in Fourier space, which also correspond to the evolutions of energy in Fourier modes, i.e., $H_{K_n}=|E_{K_n}|^2$, are shown in Fig. 8. Obviously, the large part of the energy in the system lies in the low Fourier modes. For $g=0$, the propagation of energy in all modes is periodic [14], which is consistent with the periodic recurrent solution [Fig. 3(a)]. The amplitude of the soliton structures is dominated by the total energy of system, while the width and pattern of coherent structures are associated with the energy partition in the high modes. For $g\neq 0$, however, Fig. 8 shows that the energy in the system, which is initially confined to the master mode, would spread to many slaved harmonic modes because of the nonlinear interaction, but would not regroup into the original lowest mode. The irregular

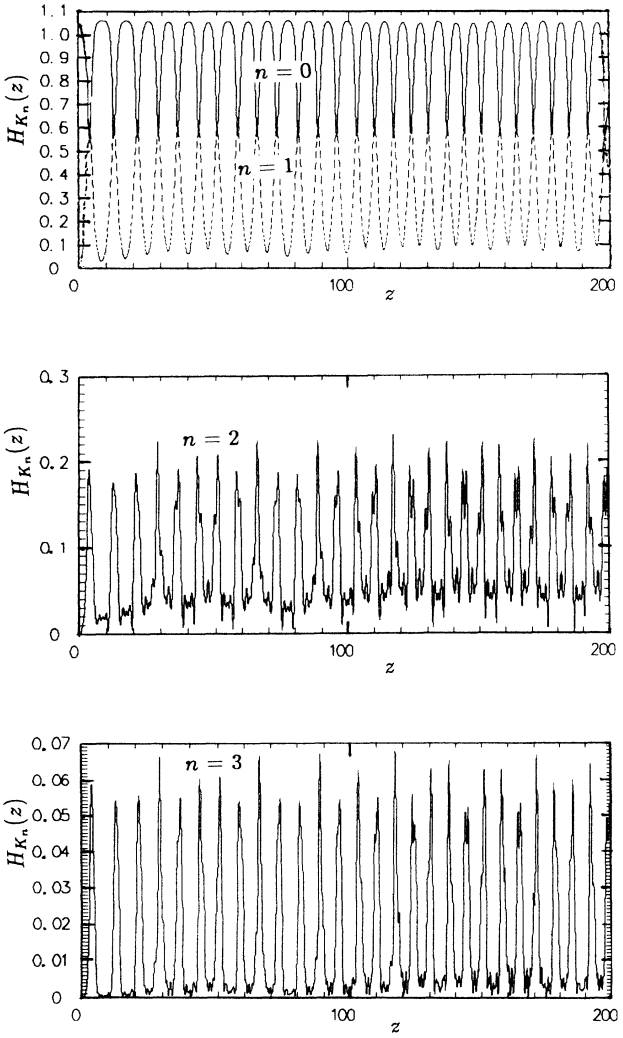

FIG. 8. Propagation of energy in the first four Fourier modes.

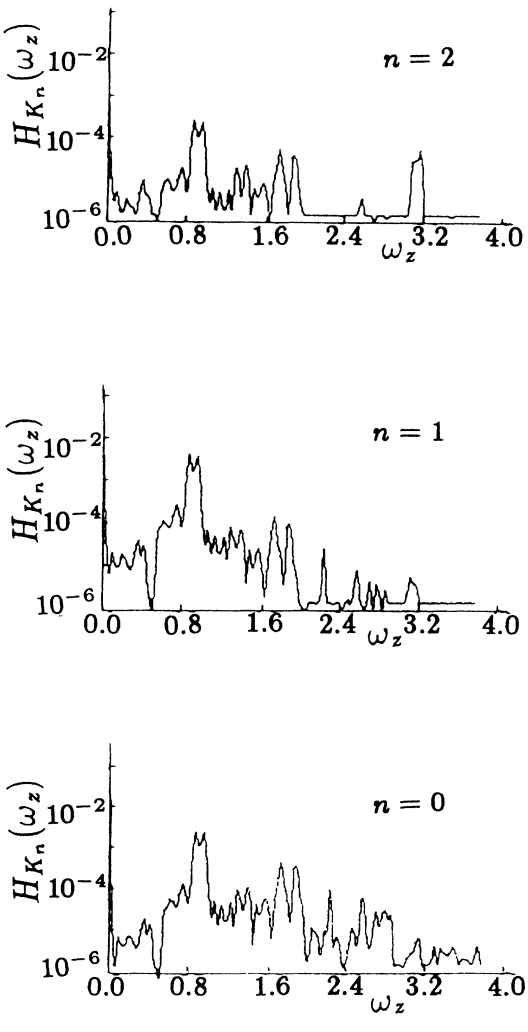

FIG. 9. The Fourier spectrum of energy ($H_{K_n}(\omega_z)\sim\omega_z$).

oscillation in the Fourier modes, in which the slaved modes interact with the master one, leads to the formation of the complicated patterns. On the other hand, we note from Fig. 9 that the power spectrum for energy in various modes is not exhibited as a clearly chaotic noise spectrum. In a sense, such a phenomenon illustrates the existence of solitarylike structures, although the well-formed structures are very irregular. In a word, the pattern dynamics is associated with the propagation of energy deposited in all Fourier modes.

V. SUMMARIES AND DISCUSSIONS

From our theoretical analysis and numerical discussions, we can summarize the main conclusions as follows. (i) The periodic solution and solitary wave solution may exist in our continuum Hamiltonian dynamic system, and the higher order saturable nonlinear effects, compared with those for the cubic term could make the amplitude and width of the light wave change. (ii) The analytical and numerical results show that nonintegrable Hamiltonian perturbation H_1 derives from the presence of chaos, where the wave field evolutions are spatially chaotic but the localized structures are still kept. (iii) The formation of the complicated patterns is associated with the stochastic partition of energy contained in Fourier modes. (iv) The route from coherent structures to complicated patterns is a quasiperiodic one.

In this research, our dynamic model, the saturable nonlinear NSE, is based on the static approximation. Speaking in terms of physics, the conditions for such an approximation to be valid are that the macroscopic length scale L must be much larger than the Debye length, macroscopic velocities must be small compared with the sound speed c_s, and macroscopic time scales must be long compared with L/c_s [3]. One should consider the light velocity to be far larger than the acoustic velocity. In fact, the response of density to the light fields is only exhibited by the nonlinear force (ponderomotive force), which corresponds to the exponential nonlinear term in Eq. (1.3). From the current investigation, we understand that such a response would lead to the stochastic propagation of light beams. On the other hand, this model has been assumed, where, for a beam pulse length much larger than the transverse spot size, the electron density is determined by the balance of ponderomotive force and electrostatic force only in the radial direction [15]. Generally speaking, the simple case of describing the light beam propagation is considered to be the axisymmetric cylindrical coordinates with $\nabla_\perp=(1/r)(\partial/\partial r)r(\partial/\partial r)$, where r is the radial variable of laser spot. Here we only deal with the case where the transverse spot consists of one variable x, which is obviously different from the real physical picture. Taking more generally physical and mathematical applications into account, however, we think that the current work is still of significance for our understanding of the propagative behavior of the light wave.

If we consider that the z variable in model (1.4) is equivalent to the evolutive time t, obviously this work exhibits the spatiotemporally chaotic dynamics of fields in the continuum Hamiltonian dynamic system, which still remains open because of the complexity of the system in the infinite degree of freedom. On the other hand, the dynamic model (1.4) can also describe the developed process of Langmuir turbulence when the variable z is replaced by the time variable t [16]. In the approximation of the weak or cubic nonlinearity, the formation of the coherent structures (solitons) can be well explained in terms of the modulational instability. But, the saturable nonlinearity has to be considered in the evolutive latter stage of plasma instability with the increase of field intensity. Our investigation also shows that the high order Hamiltonian perturbation may drive the formation of the pattern dynamics for Langmuir fields.

At last, we should mention the main difference between our work and those works that discuss the spatiotemporally complicated patterns for NSE. Until fairly recently, one studied the NSE with the driven damping, force dissipation, or nonlinear inhomogeneous media [17,18]. A rich variety of complicated patterns, which suggested that a low-dimensional chaotic attractor existed in an infinite-dimensional system, were observed. For the continuum Hamiltonian system, however, the problem becomes extremely difficult for the generally initial conditions since the system cannot be reduced to a finite-dimensional one, such as that found in the case of the dissipative perturbation, though the existence of the solitary waves could slow down the dimensions of the system. In addition, Akhmediev *et al.* only discussed the pseudorecurrence in the two-dimensional modulational instability [19], and our previous work [8] on the chaotic dynamics for the cubic-quintic NSE only described the chaotic trajectories in phase space. Here, we refer to a better description of the complicated patterns in a continuum Hamiltonian system.

One of us (C.T.Z.) wishes to acknowledge stimulating discussions with Professor S. G. Chen, and is grateful to Professor J. L. Zhang and Mr. Y. Tan for helping in numerical discussions. This work is supported by the National Natural Science Foundation of China, and in part by the CAEP foundation, Grant No. HD9317 (C.T.Z.).

[1] A. J. Schmitt, Phys. Fluids, **31**, 3079 (1988).
[2] R. L. Berger, B. F. Lasinski, T. B. Kaiser, E. A. Williams, A. B. Langdom, and B. I. Cohen, ICF Q. Rep. **2**, 77 (1992).
[3] C. E. Max, Phys. Fluids **19**, 74 (1976).
[4] J. F. Lam, B. Lippmann, and F. Tappert, Phys. Fluids **20**, 1176 (1977).
[5] P. Kaw, G. Schmidt, and T. Wilcox, Phys. Fluids **16**, 1522 (1973).
[6] T. W. Johnston (unpublished).
[7] G. Schmidt and W. Horton, Comments Plasma Phys. Controlled Fusion **9**, 85 (1985).
[8] C. T. Zhou, X. T. He, and S. G. Chen, Phys. Rev. A **46**, 2277 (1992).
[9] C. T. Zhou and X. T. He, Chin. Phys. Lett. **9**, 569 (1992).

[10] T. R. Taha and M. J. Ablowtz, J. Comp. Phys. **55**, 202 (1984).
[11] A. J. Lichtenberg, and M. A. Lieberman, *Regular and Stochastic Motion* (Springer-Verlag, Berlin, 1983).
[12] T. S. Perker and L. O. Chua, *Practical Numerical Algorithms for Chaotic Systems* (Springer-Verlag, Berlin, 1989).
[13] R. Z. Sagdeev, D. A. Usikov, and G. M. Zaslavsky, *Nonlinear Physics From the Pendulum to Turbulence and Chaos* (Harwood Academic, Chur, Switzerland, 1988).
[14] H. C. Yuen and W. E. Ferguson, Phys. Fluids **21**, 1275 (1978).
[15] G. Z. Sun, E. Ott, Y. C. Lee, and P. Guzdar, Phys. Fluids **30**, 526 (1987).
[16] P. K. Shukla, *Solitons in Plasma Physics in Nonlinear Waves,* edited by L. Debnath (Cambridge University Press, London, 1983), Chap. 11.
[17] K. H. Spatschek, H. Pietsch, E. W. Leadke, and Th. Erchermann, *Nonlinear and Turbulent Processes in Physics,* edited by V. E. Bar'yakhtar *et al.* (World Scientific, Singapore, 1989), p. 978, and references therein.
[18] T. H. Moon, Phys. Rev. Lett. **64**, 412 (1990).
[19] N. N. Akhmediev, D. R. Heatley, G. I. Stegeman, and E. M. Wright, Phys. Rev. Lett. **65**, 1423 (1990).

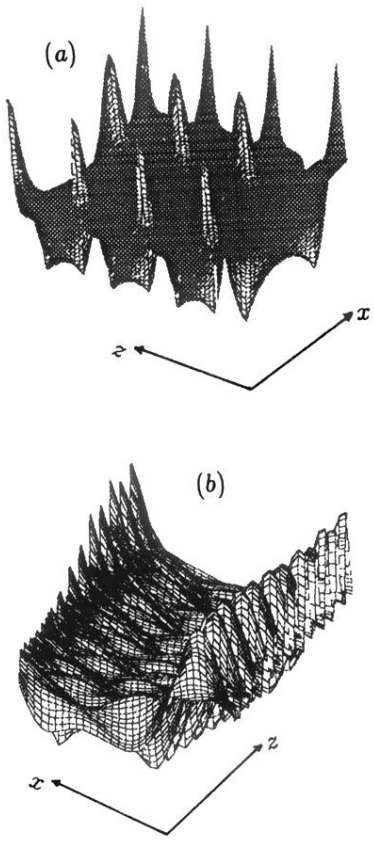

FIG. 3. Envelope amplitude of Eq. (1.4), with $\epsilon=0.1$ and $\theta=45.225°$. (a) $g=0$. (b) $g=0.1$.

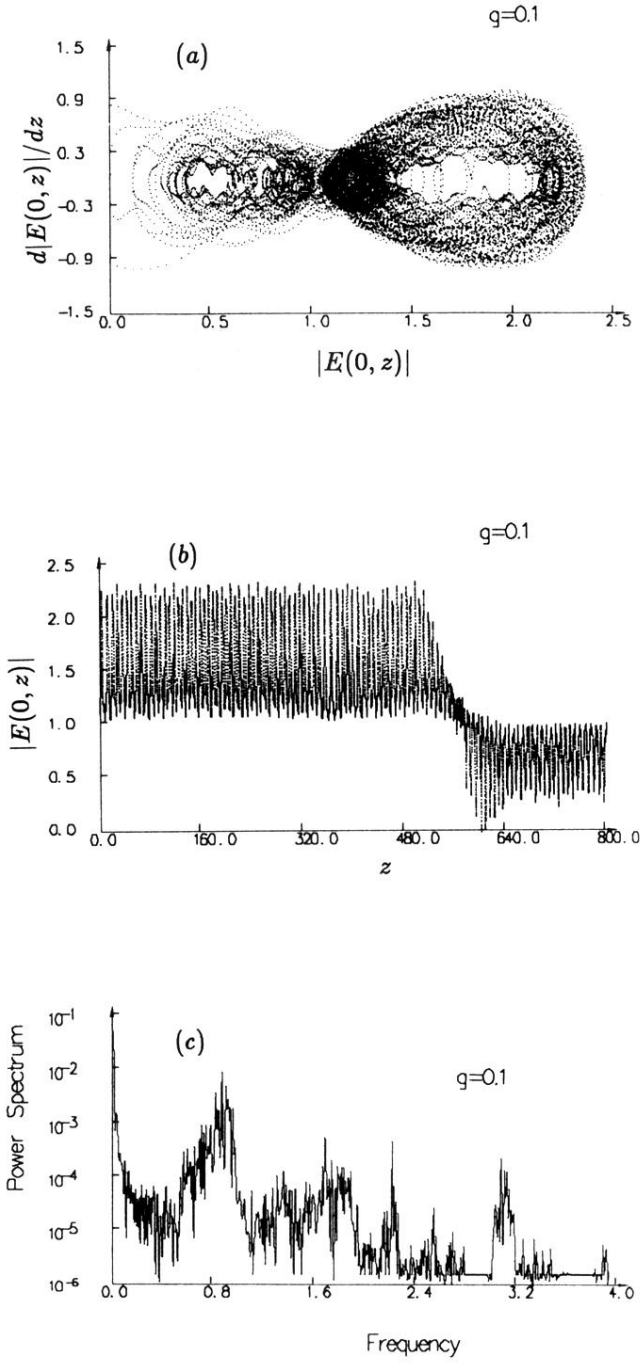

FIG. 4. (a) Phase trajectories illustrate the irregular HMO crossings. (b) Propagation of the field amplitude. (c) Continuous power spectrum shows the chaotic characteristic.